Primary cilia dysfunction as a novel pathogenic mechanism of prenatal alcohol-induced birth defects

Karen E. Boschen[1], Eric W. Fish[1], & Scott E. Parnell[1,2]*

[1]Bowles Center on Alcohol Studies, University of North Carolina, Chapel Hill, NC, USA

[2]Department of Cell Biology and Physiology, University of North Carolina, Chapel Hill, NC, USA

* Corresponding author: Scott E. Parnell, Ph.D.

Email: sparnell@med.unc.edu (SEP)

Abstract

Neurulation-stage alcohol exposure (NAE; gestational day [GD] 8-10) is associated with midline craniofacial and CNS defects that likely arise from disruption of morphogen pathways, such as Sonic hedgehog (Shh). We tested whether NAE alters Shh pathway signaling and the number and function of primary cilia, organelles critical for Shh pathway transduction. Notably, midline anomalies are also a hallmark of genetic ciliopathies such as Joubert's syndrome. Female C57BL/6J mice were administered two doses of alcohol (2.9 g/kg/dose) or vehicle on GD9. Embryos were collected 6, 12, or 24 hr later, and changes to Shh, cell cycle genes, and primary cilia were measured in the rostroventral neural tube (RVNT). At 6 and 12 hr post-NAE, reductions in Shh pathway and cell cycle gene expression and the ratio of Gli3 isoforms in the full-length activator state were observed. RVNT volume and cell layer width were reduced at 12 hr. In addition, expression of multiple cilia-related genes were observed at 6 hr post-NAE. As a further test of cilia gene-ethanol interaction, mice heterozygous for *Kif3a* exhibited perturbed behavior during adolescence following NAE compared to vehicle-treated mice, and *Kif3a* heterozygosity exacerbated the hyperactive effects of NAE on exploratory activity. These data demonstrate that NAE downregulates the Shh pathway in a region of the neural tube that gives rise to ventral midline brain structures sensitive to alcohol and suggests primary cilia dysfunction, or a "transient ciliopathy", as a cellular mechanism of prenatal alcohol pathogenesis.

Introduction

Prenatal alcohol exposure is the leading cause of preventable birth defects in the US, with Fetal Alcohol Spectrum Disorders (FASD) estimated to affect at least 5% of live births each year (1). Alcohol exposure often occurs before pregnancy is identified, during the early, important stages of embryonic development, such as gastrulation and neurulation. Early gestational alcohol exposure has been linked to growth retardation, central nervous system dysfunction, and distinct craniofacial malformations, including the “classic” facial phenotype of Fetal Alcohol Syndrome (FAS) characterized by midline defects such as hypotelorism and an absent philtrum (2, 3), as well as more subtle facial variances (4). Alcohol exposure during gastrulation, the stage when the embryo first forms distinct cell layers (3rd week in humans, gestational day [GD] 7 in mice), induces widespread cell death in the neuroectoderm (5), and subsequent diminished Sonic hedgehog (Shh) signaling as a pathogenic mechanism for gastrulation alcohol exposure (6-10). Alcohol exposure during neurulation, as the neural tube forms and closes (~4th-5th weeks in humans, GD8-10 in mice), produces midline structural defects in brain regions such as the hypothalamus, ventricles, pituitary, and septal regions (11-13), however, these defects are independent of corresponding apoptosis (5).

The Shh signaling pathway is transduced within immotile sensory organelles known as primary cilia (14, 15). Genetic disruption of the function and/or stability of primary cilia induces several developmental abnormalities, exemplified by the ciliopathy diseases, such as Joubert’s syndrome. Genetic ciliopathies cause multiple organ system defects, ocular malformations, cleft palates and lips, holoprosencephaly, and polydactyly (16, 17). Abnormal Shh signaling has been reported in cultured cells collected from humans with gene mutations linked to ciliopathies (18, 19) and knockdown of *Kif3a* or other intraflagellar transport proteins in mouse models of ciliopathies disrupts the Shh pathway (20-23) and causes Gli-dependent midfacial defects (24, 25).

We hypothesized that neurulation-stage alcohol exposure (NAE) also disrupts Shh signaling in the rostroventral region of the neural tube (RVNT) that gives rise to many of the affected midline brain

structures, explaining the manifestation of subtle craniofacial and CNS defects associated with alcohol exposure during this developmental window. We tested the effect of mid-neurulation (GD9.0) alcohol exposure on expression of the *Shh* pathway and cell cycle genes within the 12 hr following exposure. Following determination that NAE significantly decreased Shh and cell cycle gene expression, we were interested in whether primary cilia dysfunction could play a role in the Shh pathway disruption, as Shh transduction takes place within the primary cilia. To test this question, we analyzed the density of primary cilia in the RVNT and expression of genes known to play a role in cilia protein trafficking and ciliogenesis. Finally, we studied whether NAE interacts with cilia function to increase the sensitivity to the long-term effects of NAE. For this experiment, we exposed embryonic mice with a partial deletion of the key cilia gene *Kif3a*, a well-characterized mouse model of genetic ciliopathies, to GD9.0 alcohol and then during adolescence, measured behaviors that are affected by prenatal alcohol.

Methods and Materials

Animals

Male and female adult C57BL/6J mice were obtained from Jackson Laboratories (Stock No: 000664; Bar Harbor, ME). Males were housed singly and females were housed in groups of up to five per standard polycarbonate cage with cob bedding, access to a shelter, and nesting material. All mice had *ad libitum* access to food (Prolab Isopro RMH 3000, LabDiet, St. Louis, MO) and water, and were maintained on a 12:12 hr light/dark cycle. For mating, 1-2 female mice were placed into the cage of a male for 1-2 h and were checked for a vaginal plug to confirm copulation. GD0.0 was defined as the beginning of the mating session when the plug was found. Mated females were weighed and housed in a clean cage with up to 5 mice.

For behavior studies, male *Kif3a*$^{+/-}$ (B6.129-Kif3a^{tm1Gsn}/J, Stock No: 003537; Jackson Laboratories, Bar Harbor, ME) and female C57BL/6J mice were obtained, housed, and mated as described above to produce *Kif3a*$^{+/+}$ and *Kif3a*$^{+/-}$ offspring. Generation of *Kif3a*$^{-/-}$ mice was avoided as this mutation is embryonically lethal. All dams were singly housed in clean cages on GD15. Alcohol-

and vehicle-treated litters (see below) were housed with their dams, culled to a maximum of 8 pups/litter at postnatal day (PD) 3, weighed, ear marked, and tail-clipped for genotyping on PD14, and left undisturbed until weaning at PD28 when they were housed in same sex groups with their littermates. All the mice from each litter were tested on behavioral experiments conducted between PD28–33 by an experimenter who was unaware of the prenatal treatments and *Kif3a* genotype.

Neurulation-stage alcohol exposure (NAE)

On GD9.0, pregnant dams were administered two doses of ethanol (25% vol/vol ethyl alcohol, Pharmaco-Aaper, Brookfield, CT, at a dose of 2.9 g/kg) in Lactated Ringer's solution 4 hr apart via intraperitoneal (i.p.) injection. These mice were designated as the NAE group. A separate group of mice were administered an equal volume of vehicle (1.5 ml/100 g body weight). This model of alcohol exposure has been previously shown to result in maternal blood alcohol concentrations of ~400 mg/dl (26). For molecular studies, dams were humanely sacrificed via CO_2 followed by cervical dislocation either 6, 12, or 24 hr after the first ethanol injection. Embryos were dissected out and placed into cold RNase-free Dulbecco's saline solution. For all assays, embryos were age-matched based on somite number (GD9.25: 21-22 somites, GD9.5: 24-25 somites, GD10: 30-31 somites). A maximum of two embryos per litter were used in each assay to minimize litter effects.

Embryo immunohistochemistry

The chorion and amnion were removed from all embryos and they were placed into 4% paraformaldehyde for ~72 h. Stage-matched embryos were then processed for paraffin-embedding on a Leica tissue processing station. Embryos were embedded in a paraffin block and sectioned at 7 µm on a microtome. A total of 6-10 sections per embryo, encompassing the rostroventral neural tube (RVNT), were processed for immunohistochemistry. Briefly, paraffin residue was dissolved in xylenes and sections were rehydrated in ethanol washes. Slides were quenched in 10%H_2O_2/90% methanol for 10 min and incubated for 30 min in 10% Citra Plus Buffer (BioGeneX, Fremont, CA) in a steam chamber. The slides were then blocked in normal goat serum/Triton-X/bovine serum albumin blocking

solution for 1 hr and incubated overnight with primary antibody (Arl13b, 1:500, NeuroMabs, University of California-Davis) at 4°C for 24 h. Slides were then incubated with secondary antibody (anti-mouse Alexafluor 488, 1:1000, Thermofisher, Waltham, MA) for 2 hr at room temperature and cover slipped with Vectashield HardSet Antifade Mounting Medium with DAPI (Vector, Burlingame, CA).

Confocal imaging and image quantification

Cilia were imaged on a Zeiss 880 confocal microscope with a 40x oil lens. Image stacks were obtained at a step of 0.46 µm between images. Stacks were then compressed into a single image containing a depth color code with Fiji (ImageJ) software (27). Cilia within the known volume of the RVNT were counted with the Cell Counter plug-in and expressed as number of cilia per 100 μm^3. RVNT volume and cell layer width were determined using images of the same sections taken with a 10x lens. The DAPI-labeled cell layer was traced to obtain volumetric measurements and the cell layer width was measured at multiple points within each RVNT (2 measurements per slide) using Fiji software.

Gene expression assays

The RVNT of stage-matched GD9.25 embryos were dissected and placed into lysis buffer and stored at -80°C until processing. RNA was isolated from the supernatant using the RNeasy Plus Micro Kit (Qiagen, Valencia, CA). Nucleic acid concentration and quality were determined using the Qubit 3.0 fluorometer and Nanodrop 2000 (Thermofisher, Waltham, MA). Multiplex qRT-PCR was used to determine alcohol-induced gene expression changes (n = 6 embryos/treatment). Taqman probes (Invitrogen) and Taqman Multiplex PCR mix (Applied Biosystems) were used to determine expression changes in the following genes at GD9.25: *Cep41* (Mm00473478), *Hap1* (Mm00468825), *Rilpl2* (Mm01199587), *Evc* (Mm00469587), *Nek4* (Mm00478688), *Dpcd* (Mm00620237). To further investigate potential effects of alcohol on the Shh pathway and downstream transcriptional regulators, *Shh* (Mm00436528), *Gli1* (Mm00494654), and *Gli2* (Mm01293117) were analyzed using qRT-PCR at GD9.5. At GD9.25 and GD9.5, cyclin D1 (*Ccdn1*; Mm00432359), cyclin D2 (*Ccdn2*; Mm00438071), and fibroblast growth factor 15 (*Fgf15*; Mm00433278) were analyzed. For all assays, *18s* (Mm03928990) or

Pgk1 (Mm000435617) were used as reference genes. All reactions were run in triplicate and amplicon specificity was confirmed with gel electrophoresis.

Western Blot

RVNT's of each litter (n = 5-10 samples per tube) were pooled and lysed in RIPA buffer with 1X Halt protease and phosphatase inhibitors (Thermofisher, Waltham, MA) in order to obtain sufficient protein for western blot analyses. For GD9.25, 5 vehicle and 6 NAE litters were used, and for GD9.5, 6 vehicle and 7 NAE litters were used. Protein concentrations were determined with the Micro BCA kit (Thermofisher, Waltham, MA) and colorimetrics measured at 540 nm on a spectrophotometer. 15 µg of sample with 4X Laemmli sample buffer were added to each lane of a tris-glycine gel in 1X TGX running buffer and run at 150V for 45 min. Protein weights were determined with the Dual Color protein ladder (Bio-Rad, Hercules, CA). Proteins were transferred to a membrane using the iBlot2 system and incubated overnight at 4°C with primary antibody (anti-Gli3, 1:500, AF3690, R&D Systems, Minneapolis, MN). Membranes were then incubated in secondary antibody (anti-goat Alexafluor 680, 1:10,000, Thermofisher, Waltham, MA) for 1 hr at room temperature and imaged on a Licor Odyssey scanner. GAPDH (1:3000, 14C10, Cell Signaling, Danvers, MA) was used as an internal loading control. The relative intensities of the Gli3 protein bands ($Gli3^{FL}$ [~190 kDa] and $Gli3^{Rep}$ [~83 kDa]) were analyzed with ImageJ Gel Analyzer software and normalized to internal control bands. The ratio of $Gli3^{FL}$: $Gli3^{Rep}$ isoforms was calculated and expressed as a percentage of total Gli3.

Adolescent behavioral procedures

All the mice from each litter generated from the mating of a *Kif3a*$^{+/-}$ male and C57BL/6J female (n = 16 litters vehicle-exposed and 19 litters NAE) were tested on behavioral experiments conducted between PD28–33 by an experimenter unaware of the prenatal treatments and *Kif3a* genotype. The experiments were conducted in the UNC Behavioral Phenotyping Core during the light portion of the 12:12hr light:dark schedule. All mice were tested in the following testing order: rotarod trials 1-3; elevated plus maze (EPM); open-field; rotarod trials 4 and 5. The EPM was tested before the open field

to minimize potential carry-over effects, as the EPM is more sensitive to the effects of prior testing history (28, 29). Technical issues during testing resulted in two male animals being excluded from the EPM and one male from open field analyses.

The rotarod (Ugo-Basile, Stoelting Co., Wood Dale, IL) measured the latency to fall off or rotate around the top of a dowel which progressively accelerated from 3 rpm to 30 rpm during the maximum of a 5-min test, conducted during three repeated trials on the first day of testing and two repeated trials on the second day of testing. Each trial was separated by ~45 sec. The EPM was 50 cm above the floor and contained two open arms (30 cm length, 220 lux) and two closed arms (20 cm high walls, 120 lux). During the 5-min test, an observer recorded the number of entries and time spent in each of the arms. These data were used to calculate the percent of open arm time [(open arm time/total arm time) x 100], the total arm entries, and the percent of open arm entries [(open arm entries/total arm entries) x 100]. The open field (41 x 41 x 30 cm) was illuminated (120 lux at the edges, 150 lux in the center), housed within a sound-attenuated chamber and equipped with upper and lower grids of photobeams for the detection of horizontal and vertical activity and position of the mouse (Versamax System: Accuscan Instruments, Columbus, OH). The open field was conducted over 60 min and the primary measures were horizontal activity, total distance traveled, time spent in the center of the chamber, and distance traveled in the center. Number of rears and rotations were also recorded. Open field data were analyzed as four separate 15-min epochs (i.e. min 0-15, min 16-30, min 31-45, and min 46-60), based on prior findings that the initial minutes of the open field test are most sensitive to developmental drug exposure (11, 30).

Adolescent brain measurements

Following completion of behavioral tasks on PD37, mice were deeply anesthetized with tribromoethanol anesthesia and transcardially perfused with 1X PBS followed by 10% formalin. Brains were removed and stored in formalin for at least one week. Prior to paraffin embedding, fixed whole brains were cleared by rocking at room temperature in 1X PBS for one week and 70% ethanol for one

week (each solution changed daily). Brains were then cut into two sections, the frontal lobes and cerebellum, and paraffin-embedded on a Leica tissue processing station. Tissue was then embedded in paraffin block and sectioned at 10 µm on a microtome. Every 5th slide (containing 3-4 sections per slide) throughout the entirety of the cortex was stained using cresyl violet. One section per slide was imaged and the ventricles traced using Fiji/ImageJ (27). Total area of the ventricles were summed per section and averaged across the entire brain. For midline brain width and medial height, lines were drawn across images of one section of each slide throughout the cortex and measured in Fiji. Midline brain width was measured at the widest part of the cortex (dorsal/ventral bregma ~3.0) and height was measured as close to the midline as possible (medial/lateral bregma 0.25); measurements were averaged across the entire brain.

Statistical analyses

Cilia number, RVNT volume, and Western blot band intensity were analyzed using unpaired *t*-tests comparing prenatal treatment (NAE vs. vehicle) at each time point with Welch's correction when necessary. Multiplex qRT-PCR gene expression data are expressed as log2 fold change calculated using the 2-ΔΔCt method (31) and analyzed using unpaired *t*-tests with Welch's correction when necessary. The Benjamini-Hochberg correction was used if multiple unpaired *t*-tests were run within an experiment (false discovery rate = 0.10) (32). Raw *p*-values shown in tables and in the text remain statistically significant following correction unless otherwise noted. For behavior assays, litter means were analyzed for each treatment and genotype to control for between litter effects (33). Males and females were analyzed separately, because our previous studies demonstrated sex differences on these measures (11, 34, 35) . EPM data were analyzed using two-way ANOVAs (treatment x genotype) and open field and rotarod data were analyzed with three-way ANOVAs (treatment x genotype x time bin or trial). For the behavioral analysis, we predicted, *a priori*, that any effects of NAE or *Kif3a*$^{+/-}$ would be exaggerated when these treatments were combined, in other words, that the NAE *Kif3a*$^{+/-}$ mice would have the largest difference from the vehicle-treated *Kif3a*$^{+/+}$ mice. Ventricle area measurements

were analyzed using a three-way ANOVA (treatment x genotype x bregma), while width and height measurements were analyzed with two-way ANOVAs (treatment x genotype). *Post hoc* analyses were conducted when appropriate. Statistical differences were considered significant at an adjusted *p*-value threshold of 0.05.

Results

NAE downregulates expression of the Shh pathway

Previous work has demonstrated that the shape and size of the ventricles, pituitary, and hypothalamus are altered following NAE (11-13), suggesting that during neurulation the RVNT (from which these structures are derived) is particularly vulnerable to alcohol. Dysregulation of Shh signaling within the RVNT is likely a mechanism for structural changes to midline brain regions following NAE, however, this hypothesis has never been tested (36). To determine whether NAE alters the Shh pathway in the RVNT, we administered two doses of 2.9 g/kg alcohol during mid-neurulation (GD9.0) to model binge-like alcohol exposure. We collected the RVNT of stage-matched embryos 6 and 12 hr later (GD9.25 and GD9.5) and analyzed *Shh, Gli1,* and *Gli2* gene expression, relative to the housekeeping genes *Pgk1* or *18s*. First, we found that NAE significantly downregulated *Shh* at both the 6 and 12 hr time points (-0.87 and -1.89 log2 fold change, respectively; Fig 1A; Table 1), extending previously reported reductions in Shh following gastrulation-stage alcohol (9, 10) and demonstrating that NAE also impairs Shh levels in the RVNT, but is independent of concurrent apoptosis (5). Following Shh activation, Gli1 is rapidly upregulated, whereas Gli2 is constitutively expressed. However, without Shh present, Gli2 is cleaved and tagged within the primary cilium for degradation. Activation of Smoothened (Smo) by Shh deactivates this cilia-mediated cleavage of Gli2 and allows it to be shuttled outside of the cilia to activate downstream genes. Neither Gli1 nor Gli2 gene expression was altered by NAE at the 6 hr time point. However, NAE significantly downregulated *Gli1* relative to controls (-0.74 log2 fold change; Table 1, Fig 1A), but not *Gli2,* 12 hr post-exposure. In addition, we measured the relative amounts of the two forms of Gli3 protein 6 and 12 hr following the beginning of NAE. In the absence of

Shh and with normal cilia functioning, Gli3 is found predominantly in the cleaved repressor form ($Gli3^{Rep}$). Upon Shh pathway activation, the balance of $Gli3^{Rep}$ to the full-length activator form ($Gli3^{FL}$) is tipped slightly to the activator form to allow Gli1 and Gli2 to proceed with normal gene transcription, including cell cycle genes such as the cyclin family, as well as having a positive feedback effect on Shh itself. Six hr after NAE, there was no change in the ratio of $Gli3^{FL}$:$Gli3^{Rep}$ in the RVNT (59.27% $Gli3^{Rep}$ in NAE embryos vs. 62.93% $Gli3^{Rep}$ in vehicle-treated embryos, $t_{(9)} = 0.353$, $p = 0.733$; Fig 1B). However, NAE led to a significantly shifted ratio at the 12 hr time points, with a higher percentage of Gli3 in the repressor form ($Gli3^{Rep}$) compared to vehicle treatment (65.27% $Gli3^{Rep}$ in NAE vs. 54.7% $Gli3^{Rep}$ in vehicle-treated $t_{(11)} = 2.67$, $p = 0.02$; Fig 1B). No difference in total amount of Gli3 was observed between treatment groups at either time point and the amount of $Gli3^{Rep}$ did not significantly differ between the GD9.25 and GD9.5 vehicle-treated groups ($t_{(9)} = 1.049$, $p = 0.32$). Changes to Shh pathway transduction could alter the developmental trajectory of craniofacial and CNS regions derived from the RVNT by affecting normal cell proliferation, resulting in the midline defects observed in mice following NAE (11-13).

Fig 1. Neurulation-stage alcohol exposure (NAE) decreases *Shh* pathway activation in the RVNT. A) 6 and 12 hrs after NAE, embryos expressed significantly less *Shh* mRNA as compared to vehicle-treated control embryos (n = 7-9 embryos per group). 12 hr after NAE, *Gli1* gene expression was significantly reduced compared to vehicle-treated embryos (n = 7 – 9 per group). Expression of *Gli2* did not differ. Gene expression data are the log2 fold change compared to the vehicle group (expressed as 0 on the graph) ± SEM. B) The relative percentage of $Gli3^{Rep}$ to $Gli3^{FL}$ was significantly higher in NAE embryos (n = 7 litters) compared to the vehicle group (n = 6 litters) 12 hr after exposure. Data are expressed as the average $Gli3^{Rep}$ or $Gli3^{FL}$ band density expressed as a percentage of total Gli3. Below are representative bands of $Gli3^{FL}$ (190 kDa) and Gli^{Rep} (83 kDa). Full blot and loading control GAPDH (37 kDa) can be seen in S1 Fig.

Table 1. Statistical results for Shh pathway and cell cycle genes.

Gene	Associated protein	Function	Log2 Fold Change	*t*(df)	Raw *p*-value
Shh	Sonic Hedgehog	Morphogen, neural patterning	GD9.25: -0.87 GD9.5: -1.89	2.741(14) 3.608(14)	0.0159* 0.0029*
Gli1	GLI Family Zinc Finger 1	Transcription factor	GD9.25: 0.01 GD9.5: -0.74	0.257(14) 2.418(14)	0.801 0.0298*
Gli2	GLI Family Zinc Finger 2	Transcription factor	GD9.25: 0.698 GD9.5: 0.035	0.293(14) 0.303(14)	0.7737 0.7667
Ccnd1	Cyclin D1	Cell cycle	GD9.25: -0.387 GD9.5: -0.62	1.781(15) 4.027(12)	0.0952 0.0017*
Ccnd2	Cyclin D2	Cell cycle	GD9.25: -0.3288 GD9.5: -0.29	1.026(15) 1.514(9.03)	0.3211 0.1637
Fgf15	Fibroblast Growth Factor 15	Cell growth	GD9.25: -1.107 GD9.5: -0.25	2.805(15) 1.103(8.14)	0.0133* 0.3017

* = Remain significant following correction for multiple comparisons.

NAE downregulates cell cycle gene expression and decreases RVNT volume

One of the outputs of the Shh signaling pathway is the expression of cell cycle genes. Based on the observed decreases in *Shh* and *Gli1* gene expression and altered $Gli3^{FL}$:$Gli3^{Rep}$ following NAE, we hypothesized that NAE would also lead to altered expression of genes involved in regulation of cell proliferation. To assess changes in Shh-mediated gene expression, we analyzed three cell cycle genes downstream of Shh: *Ccnd1*, *Ccnd2*, and *Fgf15* 6 and 12 hr following NAE. In accordance with the alcohol-induced reductions in *Shh*, *Fgf15*, but not *Ccnd1* or *Ccnd*2, was significantly downregulated 6

hr post-exposure (-1.107 log2 fold change; Fig 2A, Table 1). *Ccnd1* expression did show a trend towards a downregulation in expression (p = 0.0952). Fibroblast growth factor 15 (encoded by *Fgf15*; homologous to *Fgf19* in humans) is dependent on Shh signaling and largely overlaps with Gli1 in expression patterns early in development (37, 38). Functionally, FGF15 promotes cell cycle exit and differentiation of neuronal precursors (39). *Ccnd1,* but not *Ccnd2* or *Fgf15,* was downregulated at GD9.5 (-0.62 log2 fold change; Fig 2A, Table 1). Cyclin D1 (encoded by *Ccnd1*) regulates progression of the G1 phase of the cell cycle (40) and *Ccnd1* is activated by the Shh pathway Gli family of transcription factors (41, 42). Furthermore, Cyclin D1 is important for expansion of ventral neural precursors in the early mouse diencephalon (37).

Fig 2. NAE decreases expression of *Fgf15* and *Ccnd1* in the RVNT. A) *Fgf15* and *Ccnd1*, key Shh-mediated factors important for cell proliferation processes, were downregulated compared to vehicle-treated control embryos (n = 6-8 embryos per group) at 6 and 12 hr post-exposure, respectively. B) RVNT volume is significantly reduced in NAE embryos (filled bars, n = 7) compared to vehicle-treated embryos (open bars, n= 9) 12 hr after exposure, but did not differ at the other two time points. GD10 RVNTs were also significantly larger than both GD9.25 and GD9.5. C) Cell layer width did not differ based on prenatal treatment but did increase over time, with GD10 embryos exhibiting wider RVNT cell layers compared to both GD9.25 and GD9.5 embryos. ** = $p < 0.01$, *** = $p < 0.001$, **** = $p < 0.0001$, all values expressed as mean + SEM.

Given the disruption of cell cycle-related gene expression, we next analyzed the volume of the RVNT 6, 12, and 24 hr after NAE to examine how the size of this region changed over time and in response to alcohol (Fig 2B). Images taken from the RVNT were obtained at 40x for volumetric analyses; section thickness was also measured at 40x. A significant time (hours post-exposure) x treatment interaction was observed ($F_{(2,39)} = 6.164$, $p = 0.0047$), as well as main effects of both time ($F_{(2,39)} = 22.08$, $p < 0.0001$) and treatment ($F_{(2,39)} = 5.018$, $p = 0.031$). As expected, the volume of the RVNT increased across time, with GD10 embryos having significantly larger RVNTs compared to both GD9.25 ($p < 0.0001$) and GD9.5 ($p = 0.0002$), demonstrating the exceptional growth of the neural tube

over this period. There was a trend towards GD9.5 embryos being larger than GD9.25 (p = 0.065), however this relationship was not significant. Importantly, RVNT volume was significantly smaller in NAE compared to vehicle-treated embryos (0.197 mm^3 vs. 0.3224 mm^3) on GD9.5 (p = 0.0085) and tended to be smaller on GD10 as well, though this difference did not reach statistical significance (p = 0.1). The thickness of the RVNT cell layer was also assessed, however while the cell layer did grow thicker across time ($F_{(2,39)}$ = 9.142, p = 0.0006), there was no significant effect of treatment (Fig 1C). GD10 embryos had increased widths compared to both GD9.25 (p = 0.0049) and GD9.5 (p = 0.0012). The increase in cell layer width corresponds to the larger overall volume at GD10. The rapid changes in RVNT volume across the first 24 hr post-alcohol exposure indicate that significant structural changes are taking place and encourages further investigation into all factors by which alcohol could affect growth, including alterations to cell proliferation. Even transient growth inhibition within this region of the neural tube could have long-lasting consequences on brain development.

NAE alters expression of key cilia-related genes, but not cilia density in the RVNT

Shh transduction occurs within the axoneme of primary cilia, nearly ubiquitous structures of mammalian cells that play a particularly important role during embryonic development. Dysregulation of RVNT primary cilia poses a risk to the normal development of brain regions that arise from this area of the neural tube, namely midline structures such as the hypothalamus, septum, pituitary, and preoptic area (43), many of which have been shown to be altered by NAE (11-13). Additionally, midline anomalies such as hypertelorism are a hallmark of genetic ciliopathies and have also been reported in a subset of patients with heavy prenatal alcohol exposure (4), suggesting an overlapping etiology between ciliopathies and prenatal alcohol.

Based on the reduction in *Shh* and downstream cell cycle gene expression, we hypothesized that we might find a coinciding NAE-induced change in either 1) the number of primary cilia or 2) cilia-related genes in the RVNT. First, we examined the direct impact of NAE on primary cilia in the RVNT

by analyzing cilia density. Primary cilia were labeled for the cilia-specific small GTPase Arl13b at 6, 12, or 24 hr following NAE (Fig 3A) and the number of cilia within the known volume of the RVNT were analyzed using 3D image stacks from confocal images. A significant time (hours post-exposure) x treatment interaction was found ($F_{(2,39)} = 3.642$, $p = 0.036$), as well as a main effect of time ($F_{(2,39)} = 18.93$, $p < 0.0001$) (Fig 3B). No main effect of treatment was observed. No significant differences were seen between vehicle and NAE embryos at any time point, though there was a trend towards an increase in cilia density at the GD9.5 (12 hr post-exposure) time point ($p = 0.087$). The density of cilia in the RVNT significantly decreased over time, as there was a higher density of cilia at GD9.25 compared to both GD9.5 and GD10 ($p < 0.0001$ for both time points). This reduction in density is likely due to the substantial growth of the neural tube during neurulation (Fig 2B-C), however the lack of a treatment effect precludes alcohol-induced effects on cilia number as the mechanism of action of reduced cell cycle gene expression. The lack of alcohol-related effect rules out cilia number as a primary mechanism and identifies cilia function as a more likely driver of NAE effects.

Fig 3. NAE alters expression of cilia-related genes in the RVNT but does not alter cilia density. A) Primary cilia in the RVNT at GD9.5 were labeled with an anti-Arl13b antibody (green). Scale bar = 10 µm. B) Cilia density did not differ at any of the time points, but did decrease across time points, as GD9.5 and GD10 had lower cilia density compared to GD9.25 (n = 6-9). ** = $p < 0.01$, **** = $p < 0.0001$, all values are expressed as mean + SEM. All gene expression data are the log2 fold change compared to the vehicle group (expressed as 0 on the graph) ± SEM. C) NAE resulted in significant changes to expression levels of genes related to ciliogenesis, post-transcriptional modification to ciliary tubulin, and genes implicated in genetic ciliopathies 6 hr after exposure. At 12 hr post-exposure, all genes had returned to baseline expression levels except for *Dpcd*, which remained significantly downregulated. Encoded proteins associated with these genes can be found in Table 2. For all genes, n = 6-8 embryos per group. * = $p < 0.05$, ** = $p < 0.01$. Data are expressed as log2 fold change compared to the vehicle group (expressed as 0 on the graph) ± SEM.

We further investigated primary cilia homeostasis and stability through analysis of cilia-related genes 6 hr following NAE. This time point was chosen to allow us to investigate differential gene expression that preceded, and likely led to, the reductions in the Shh pathway and RVNT volume. Six genes of interest (*Hap1*, *Rilpl2*, *Cep41*, *Nek4*, *Evc*, and *Dpcd*) were identified by comparing a previously generated RNA-seq data set (44) and the cilia gene database Cildb (45, 46) (Table 2, Fig 3C). Notably, these genes are either mutated in human genetic ciliopathies or shown to play an important role in ciliogenesis, ciliary protein trafficking, or cilia stability through maintenance of post-translational modification. Expression patterns of these genes were analyzed 6 and 12 hr after NAE using qRT-PCR. At GD9.25, NAE upregulated two of the genes, *Hap1* and *Rilpl2* (1.19 and 0.37 log2 fold change, respectively), in the RVNT (Table 2; Fig 3C). Both *Hap1* and *Rilpl2* are associated with ciliogenesis (47, 48), with *Ripl2* also playing a role in ciliary protein transport (48). *Hap1* is named for its role in Huntingtin's disease. *Hap1* has been shown to mediate ciliogenesis through interaction with Huntingtin (Htt) (47). While little is known regarding ciliopathies in patients with Huntington's disease, patients with Huntington's and mice with introduction of mutated Htt exhibit abnormally increased cilia number and length (47, 49). In addition, mutated Htt disrupts the normal binding of Hap1 to dynein, affecting protein transport (50). Increased expression of ciliogenesis-related genes could be a result of alcohol-induced disruptions of normal cell cycle progression in the RVNT, as cilia are retracted and extended during mitosis. However, any changes to ciliogenesis driven by these genes are transient, as expression levels returned to baseline by GD9.5 (Table 2, Fig 3C).

In contrast, the last four genes (*Cep41*, *Nek4*, *Evc*, and *Dpcd*) showed marked downregulation 6 hr following NAE (GD9.25) (Table 2, Fig 3C). The first, *Cep41* (-1.61 log2 fold change), is known to be mutated in patients with the genetic ciliopathy Joubert's syndrome (51). Patients with Joubert's display many symptoms similar to other ciliopathies, including renal, ocular, digital, and neurological abnormalities. Notably, patients with Joubert's also show clinical symptoms that overlap with some features of FASD, including cerebellar dysplasia, impaired motor function, abnormal eye development, polydactyly, and craniofacial dysmorphologies. In mouse and zebrafish models, loss of *Cep41* causes

ciliopathy-like phenotypes, including brain malformations (51). Thus, even transient downregulation of this gene could impact normal CNS development. In addition, Cep41 is implicated in polyglutamylation of ciliary α-tubulin; loss of tubulin glutamylation could result in structural instability and possibly affect ciliary assembly and transport. Further studies are needed to determine if changes to *Cep41* expression are directly linked to glutamylation status of ciliary tubulin in the RVNT following NAE. *Nek4* was also downregulated following NAE (-0.45 log2 fold change). Ciliary assembly and integrity are in part mediated through *Nek4*, possibly through *Nek4*'s regulation of microtubules (52). The gene *Dpcd* (-0.4 log2 fold change) is associated with another ciliopathy, Primary Ciliary Dyskinesia, caused by dysfunction of motile cilia in the respiratory tract and reproductive systems, resulting in respiratory difficulties and infertility (53). *Dpcd* has been implicated in the formation and maintenance of cilia and is upregulated during cell division. Finally, downregulation of *Evc* (-0.43 log2 fold change) could have direct impact on trafficking of the Shh pathway proteins Smo and the Gli family (54, 55). Ellis-van Creveld syndrome, caused by a mutation in *Evc*, is a genetic ciliopathy presenting with polydactyly and other digital anomalies, congenital heart defects, and other skeletal abnormalities. Similar skeletal malformations have been noted in humans and rodent models of FASD (56-58). *Dpcd* remained significantly downregulated (-0.467 log2 fold change; Table 2, Fig 3C) 12 hr after NAE; however, expression of *Cep41*, *Nek4*, and *Evc* had returned to control levels. A schematic of cilia genes altered following NAE at 6 and 12 hr is shown in Fig 4. In summary, NAE results in changes to gene expression related to cilia function, stability, and ciliogenesis that coincide with and precede downregulation of important morphogenic and cell proliferation pathways.

Table 2. Statistical results for cilia-related genes.

Gene	Associated protein	Function	Log2 Fold Change	*t*(df)	Raw *p*-value
Hap1	Huntingtin-associated Protein 1	Ciliogenesis	GD9.25: 1.19 GD9.5: 0.448	3.364(10) 1.034(16)	0.0072* 0.3166
Rilpl2	Rab-Interacting Lysosomal Protein-Like 2	Ciliogenesis, protein trafficking	GD9.25: 0.37 GD9.5: -0.039	2.567(10) 0.238(18)	0.0281* 0.814
Cep41	Centrosomal Protein 41	Post-translational modifications of ciliary tubulin	GD9.25: -1.61 GD9.5: -0.179	3.675(13) 0.688(17)	0.0057* 0.501
Nek4	NIMA Related Kinase 4	Cell cycle, cilia function	GD9.25: -0.45 GD9.5: -0.048	2.361(14) 0.236(18)	0.033* 0.816
Dpcd	Deleted In Primary Ciliary Dyskinesia Homolog (mouse)	Generation and maintenance of ciliated cells	GD9.25: -0.40 GD9.5: -0.467	2.711(13) 2.389(19)	0.0178* 0.0274*
Evc	Ellis-van Creveld syndrome protein homolog (mouse)	Localized to cilia, interacts with Smo, Gli trafficking	GD9.25: -0.43 GD9.5: -0.175	2.548(14) 0.565(15)	0.0232* 0.5801

* = Remain significant following correction for multiple comparisons.

Fig 4. Schematic of a primary cilium. This representation of the primary cilium includes the axoneme, basal body, and centriole and displays differentially expressed genes related to cilia structure/ciliogenesis/protein trafficking at GD9.25 (6 hr post-exposure) and the Shh pathway and cilia function at GD9.5 (12 hr post-exposure). Orange outlines indicate upregulated genes whereas blue outlines denote genes that were downregulated by NAE.

Partial knockdown of cilia gene Kif3a interacts with NAE to affect adolescent behavior

To further test the hypothesis that cilia dysfunction is a mechanism for the consequences of NAE, we utilized a transgenic mouse strain with a partial deletion of *Kif3a*, a gene that codes for an

intraflagellar transport protein. Full deletion of *Kif3a*, is a well-characterized ciliopathy model (24, 59, 60), and if cilia dysfunction was involved in the effects of NAE, then *Kif3a* heterozygosity would both phenocopy and exacerbate NAE. We focused on a NAE effect that we have previously shown to be robust and reproducible, behavioral change during adolescence (11). Adolescent male and female mice exposed to GD9.0 alcohol were tested on a battery of behavioral tasks, but since the largest behavioral changes occurred in males, we discuss behavior from male, rather than female, mice in detail (for female data refer to Fig S2B, S3A-D; S1 Table). Sex-specific effects of early gestational alcohol have been previously reported to emerge in adolescence and adulthood and likely result from postnatal sex differences, as opposed to embryonic effects of alcohol (11, 34, 35, 61).

We first examined motor coordination, using an accelerating rotarod performance across five repeated trials. Although rotarod performance for all mice improved from the first to the fifth trial ($F_{(4,192)} = 28.4$, $p < 0.0001$), NAE persistently impaired motor coordination, as revealed by a main effect of NAE, regardless of *Kif3a* genotype ($F_{(1,48)} = 5.1$; $p = 0.028$; Fig S2). These results indicate that primary cilia are not critical for the motor incoordination effects of NAE. This finding is not surprising as previous research has suggested that the etiology of alcohol-induced cerebellar deficits arising from NAE is likely alcohol-induced apoptosis in the rostral rhombic lip, from which the cerebellum arises (5).

However, when we examined elevated plus maze (EPM) exploration, a two-way ANOVA found a significant genotype x treatment interaction ($F_{(1,49)} = 6.9$; $p = 0.01$),) on total arm entries. Vehicle-treated *Kif3a*$^{+/-}$ and NAE *Kif3a*$^{+/+}$ mice were more active than were vehicle-treated *Kif3a*$^{+/+}$ mice ($p = 0.006$ and $p = 0.04$, respectively) (Fig 5A), while NAE *Kif3a*$^{+/-}$ had comparably high levels of activity but were not statistically different from vehicle-treated *Kif3a*$^{+/+}$ mice ($p = 0.061$). This result replicates our previous findings on early NAE (11) and indicates that *Kif3a* heterozygosity phenocopies a locomotor hyperactivity caused by NAE. Supporting the hypothesis that NAE and *Kif3a*$^{+/-}$ also affect anxiety-like behavior, there was a significant genotype x treatment interaction on the percentage of open arm time ($F_{(1,49)} = 3.9$; $p = 0.05$) (Fig 5B), but not the percent of open arm entries (Fig 5C). *Post ho*c analysis revealed that both vehicle-treated and NAE *Kif3a*$^{+/-}$ mice spent a greater percentage of time on the

open arms than did the vehicle-treated *Kif3a*$^{+/+}$ mice ($p < 0.001$ and $p = 0.01$, respectively). Although NAE in *Kif3a*$^{+/+}$ tended to phenocopy *Kif3a*$^{+/-}$ on the open arm time, this effect was not significant in the *post hoc* analyses. To test whether NAE alone affects open arm time in the *Kif3a*$^{+/+}$ mice and confirm our previous results using a two-sample t-test (11, 34), we ran this same statistical analysis ($t_{(20)} = 3.0$; $p = 0.007$; Fig 5B) and found that that early NAE increases the percent of time on the open arms. Overall, these results indicate that NAE and *Kif3a* heterozygosity phenocopy each other's effects on the EPM.

Fig 5. Partial loss of cilia motor transport gene *Kif3a* phenocopies and potentiates the effect of NAE on behavioral performance in adolescent male mice. A) Vehicle-treated *Kif3a*$^{+/-}$ and NAE WT mice made significantly more arm entries on the EPM than did vehicle-treated WT mice. B) Vehicle-treated and NAE *Kif3a*$^{+/-}$ mice spent a greater percentage of time on the open arms than did the vehicle-treated WT mice. C) Percent of entries into the open arms was not significantly affected by genotype or treatment. D-F) Significant ($p < 0.05$) *post hoc*'s are shown as letters on each graph. a: vs. vehicle-treated WT, b: vs. vehicle-treated *Kif3a*$^{+/-}$, c: vs. NAE WT. D) A significant genotype x treatment interaction was found, indicated by the square bracket. NAE *Kif3a*$^{+/-}$ mice were more active than vehicle-treated WT mice during all four 15-min time bins. NAE *Kif3a*$^{+/-}$ mice were more active than NAE WT mice during the 2nd and 4th time bins and more active than vehicle-treated *Kif3a*$^{+/-}$ mice during the final time bin. NAE *Kif3a*$^{+/-}$ mice had more total beam breaks compared to the NAE WT and vehicle *Kif3a*$^{+/-}$ mice ($p = 0.001$ and 0.003, respectively). E) A main effect of treatment was observed, indicated by the lines and bracket, as NAE mice traveled further in the center compared to vehicle-treated mice. In addition, the total distance traveled by NAE *Kif3a*$^{+/-}$ mice was significantly more than that traveled by the NAE WT or vehicle *Kif3a*$^{+/-}$ groups ($p = 0.002$ and 0.015, respectively). F) A main effect of treatment was found, indicated by the lines and bracket, with NAE animals spending more time in the center of the chamber compared to vehicle-treated mice across time, and NAE *Kif3a*$^{+/-}$ mice spending more time in the center compared to both NAE WT and vehicle *Kif3a*$^{+/-}$ mice ($p = 0.006$ and 0.003, respectively). For all groups, n's = 11-15 litters, with same genotype littermates averaged into a single datum for each

litter. For all graphs, * = $p < 0.05$, ** = $p < 0.01$, *** = $p < 0.001$. All data are shown as group means + SEM (vehicle as open bars, NAE as filled bars).

Since the EPM is a relatively brief exposure to a complex novel environment and our procedure did not assess habituation to the maze, we further measured exploratory behavior and activity in an open field test across a 1 hr period. When initially analyzing overall horizontal activity, a three-way mixed ANOVA found a significant genotype x treatment x time bin interaction ($F_{(3,141)} = 4.3$; $p = 0.006$) (Fig 5D). *Post hoc* analysis revealed that NAE *Kif3a*$^{+/-}$ mice were more active than vehicle-treated *Kif3a*$^{+/+}$ mice during each of the 15-min time bins ($p = 0.002$, 0.001, 0.032, and 0.046, respectively), and were more active than NAE *Kif3a*$^{+/+}$ mice during the 2nd and the final 15-min time bins ($p = 0.018$ and 0.006, respectively). NAE *Kif3a*$^{+/-}$ mice were also more active than vehicle-treated *Kif3a*$^{+/-}$ mice during the final 15-min time bin ($p = 0.013$). Since the persistently high activity of the NAE *Kif3a*$^{+/-}$ mice suggests impaired habituation, we calculated a habituation index, expressing data from each 15-min time bin as a percentage of the initial time bin (i.e. min 0-15). A significant 3-way interaction (genotype x treatment x time bin; $F_{(3,141)} = 2.0$; $p = 0.039$) revealed that while all groups reduced their activity over the hour, in the final time bin, NAE *Kif3a*$^{+/-}$ mice were significantly less habituated than were the vehicle-treated *Kif3a*$^{+/-}$ mice and the NAE *Kif3a*$^{+/+}$ mice ($p = 0.02$ and 0.03, respectively). These groups had an initial bout of heightened activity, relative to the vehicle-treated *Kif3a*$^{+/+}$ mice, but NAE *Kif3a*$^{+/-}$ mice maintained a higher level of activity throughout the test.

There were significant main effects of NAE on several specific measures of activity, including repeated beam breaks ($F_{(1,47)} = 4.1$; $p = 0.05$, not shown), center distance ($F_{(1,47)} = 9.4$; $p = 0.004$, Fig 5E), and center time ($F_{(1,47)} = 12.5$; $p = 0.001$, Fig 5F). *Kif3a*$^{+/-}$ genotype also had significant effects upon repeated beam breaks ($F_{(1,47)} = 5.2$; $p = 0.03$, not shown), center distance ($F_{(1,47)} = 10.6$; $p = 0.002$, Fig 5E), and center time ($F_{(1,47)} = 7.4$; $p = 0.009$, Fig 5F) Both NAE and *Kif3a*$^{+/-}$ genotype significantly affected the number of rears, rotations, and total distance (statistics shown in S2 Table). On each of these measures, NAE *Kif3a*$^{+/-}$ mice were the most active treatment group indicating an additive effect of *Kif3a* genotype and NAE.

To further illustrate the heightened activity of the NAE *Kif3a*$^{+/-}$ mice relative to the other groups, as predicted by our hypothesis, we analyzed overall horizontal activity (Fig 5D), center distance (Fig 5E), and center time (Fig 5F) as 60-min totals and used Bonferroni *post hoc* tests to compare NAE *Kif3a*$^{+/-}$ to NAE *Kif3a*$^{+/+}$ mice (effect of genotype within NAE mice) or vehicle *Kif3a*$^{+/-}$ mice (effect of NAE within the heterozygotes), vehicle *Kif3a*$^{+/-}$ to vehicle *Kif3a*$^{+/+}$ (effect of genotype alone), and NAE *Kif3*a$^{+/+}$ to vehicle *Kif3a*$^{+/+}$ mice (effect of NAE within the wild-types). The NAE *Kif3a*$^{+/-}$ mice were more active than their NAE *Kif3a*$^{+/+}$ littermates (p = 0.001 for horizontal activity, 0.002 for center distance, and 0.006 for center time), and the vehicle *Kif3a*$^{+/-}$ mice (p = 0.003 for horizontal activity, 0.015 for center distance, and 0.003 for center time). There were no significant effects of NAE or *Kif3a*$^{+/-}$ alone. The heightened overall activity levels, as well as activity specific to the center of the open field which may reflect altered anxiety-like behavior, confirm our prior results from early NAE that open field activity is a sensitive index for the effects of early gestational alcohol exposure (11, 34). The greater sensitivity of the *Kif3a*$^{+/-}$ in the open field versus the EPM is likely due to differences in the test duration because the differences between treatment and genotype groups appear to become greater as exploration patterns adapt to the environment.

Brain width and ventricle area were also analyzed in a subset of adolescent male mice (n = 4-5 per group) chosen based on performance closest to the group means on open field horizontal activity. Neither genotype nor prenatal treatment significantly affected ventricle area, though *Kif3a*$^{+/-}$ mice tended to have larger ventricles ($F_{(1,13)}$ = 3.767, p = 0.0743; Fig S4A). A genotype-treatment interaction was found for midline brain width ($F_{(1,13)}$ = 9.206, p = 0.0096; Fig S4B), as well as a main effect of treatment ($F_{(1,13)}$ = 27.55, p = 0.0002). Dunnett's multiple comparison test was used to compare each group to vehicle-treated *Kif3*a$^{+/+}$ animals, and it was determined that the brains in all three other groups were narrower (vs. *Kif3a*$^{+/+}$ NAE: p = 0.0001; vs. *Kif3a*$^{+/-}$ Veh: p = 0.0308; vs. *Kif3a*$^{+/-}$ NAE: p = 0.0018). In addition, a main effect of genotype was found for medial brain height, with *Kif3a*$^{+/-}$ mice having shorter medial height compared to *Kif3a*$^{+/+}$ mice ($F_{(1,13)}$ = 6.332, p = 0.0258; Fig S4C). Thus, the partial deletion of *Kif3a* resulted in smaller brains in adolescence that coincided with behavioral abnormalities.

Discussion

The studies described here demonstrate that NAE disrupts the Shh pathway and cell cycle gene expression, and causes a reduction in RVNT volume during the first 12 hr following exposure. In addition, NAE disrupts expression of genes related to ciliogenesis and protein trafficking (Fig 5). Finally, cilia gene-alcohol interactions were further demonstrated through the use of *Kif3a* transgenic mice, a model of genetic ciliopathies (59). NAE male *Kif3a*$^{+/-}$ exhibited exacerbated behavioral impairments on the open field and EPM compared to controls and WT NAE mice, implicating cilia in specific behavioral deficits. The current results support that early gestational alcohol exposure disrupts the Shh pathway and suggests a primary cilia dysfunction that contributes to the development of craniofacial and midline CNS defects. Additionally, these data have implications beyond the embryonic period and the neural tube, including informing the emerging study of enhanced cancer risk in human alcoholics. Dysregulation of the developmental signaling pathways, such as Shh, contribute to cancer pathogenesis (62) and more research is focusing on primary cilia dysfunction as a mediating factor in cancer development (63).

NAE disrupts the Shh pathway and cilia function in the neural tube

These studies confirm that NAE downregulated Shh pathway expression, similar to other FASD models targeting early points of gestation (6-10). We observed decreased *Shh* expression in the RVNT of NAE embryos 6 hr post-exposure (GD9.25) and downregulated *Shh* and *Gli1* and increased levels of the Gli3^{Rep} isoform 12 hr following NAE. These data are the first to report altered Shh signaling following alcohol exposure during neurulation. While *Gli2* gene expression was not affected by NAE at either time point, it is possible that the ratio of protein isoforms was altered by NAE while not impacting levels of mRNA, similar to what was found for Gli3. Like Gli3, Gli2 is found in full-length activator and cleaved repressor forms, though studies have suggested that Gli2 acts primarily as a transcriptional

activator in the mouse neural tube (64-66), meaning the majority of Gli2 will be found in the full-length form. However, currently available antibodies cannot reliably identify these isoforms, in part due to the dearth of antibodies that bind to the correct epitope of the protein to allow for detection of the cleaved repressor (N-terminus). It will be possible to address this question once validated antibodies targeting different amino acid sequences of mouse Gli2 become available. At GD9.5, decreases in the Shh pathway activation were concomitant with smaller RVNT volume and decreased *Ccnd1*, a pro-proliferative protein downstream of the Shh pathway. The difference in the timing of NAE's impact on *Fgf15* and *Ccnd1*, in combination with the lack of effect in Ccnd2 expression, indicate possible differences between these molecules in alcohol sensitivity or expression patterns within the neural tube. Regardless, it is likely that the observed reduction in RVNT volume is due to decreased cell proliferation, not increased cell death. While not directly assessed in the current study, previous work has shown little to no excessive apoptosis in the rostral basal or floor plates of the neural tube following GD 9.0 alcohol exposure (5), in contrast to pronounced apoptosis throughout the neuroectoderm following exposure at earlier time points. In addition, it is possible that reduced activation of the Shh pathway in the ventral neural tube, however transient, allows for redistribution of morphogens and increased expression of Wnt within the dorsal neural tube. Since the dorsal neural tube also contributes to craniofacial development through Wnt and Bmp signaling, an imbalance in the morphogenic gradients would likely result in abnormal growth trajectories of regions arising from these portions of the neural tube.

The Shh pathway requires properly functioning primary cilia. While cilia density was not affected in the current study, cilia function, as identified by changes in cilia-related genes that emerge within the first 6 hr following alcohol exposure and extend to the Gli family of transcription factors after 12 hr, was significantly impaired by NAE. These data demonstrate NAE rapidly dysregulates primary cilia and identifies ciliogenesis, cilia function, and maintenance of cilia stability as targets of NAE. The decrease in *Cep41* was particularly interesting, as polyglutamylation of tubulin is important for protein trafficking within the cilia, including Shh pathway proteins (67). In addition, *Evc* is known to play a role in Gli

protein trafficking (54). Together, the downregulation of these two genes suggests disruption of Gli signaling within the cilia as a likely mechanism for the later reduction in *Ccnd1* expression. The observed downregulation of *Dpcd,* a gene normally upregulated during cilia formation and cell division, suggests that the cell cycle has already begun to be affected by NAE 6 and 12 hr post-exposure. Transient changes in cell proliferation in this region of the neural tube would impact brain and craniofacial development and manifest as anomalies phenotypically similar between FASD and genetic ciliopathies (4, 11-13).

NAE interacts with cilia dysfunction to alter exploratory behavior during adolescence

Mice lacking one copy of the *Kif3a* gene were used to demonstrate that prenatal alcohol interacts with cilia function. The *Kif3a* mutant mouse is a well-characterized model of genetic ciliopathy (59, 60, 68), as *Kif3a* mutant mice phenocopy many human ciliopathies, including hypertelorism, facial clefting, and brain abnormalities (59, 69). NAE mice can exhibit abnormal cortical hemispheres and ventral midline brain structures (12, 13), similar to the defects seen in conditional *Kif3a* mutant mice, and hypertelorism has been reported in some patients with heavy prenatal alcohol exposure who lack the classic FAS facial features (4, 70). In the current study, exploratory behavior in two novel environments (EPM and open field), which relies heavily on the cortico-limbic and hypothalamic circuitry derived from the RVNT, was sensitive to both NAE and *Kif3a* genotype effects, as well as NAE-genotype interactions. NAE and *Kif3a*$^{+/-}$ similarly increased total activity on the EPM and in the open field, a phenocopy that suggests a common mechanism. Importantly, the persistence of hyperactivity and impaired open field habituation observed in the NAE *Kif3a*$^{+/-}$ mice supports the hypothesis that a primary cilia dysfunction is a risk factor for certain behavioral effects of NAE. In addition to overall motor activity, heightened exploration of the EPM open arms and the center of the open field suggest an impaired stress and or anxiety-related response, as previously observed following gestational alcohol exposure (35).

Conclusions

In conclusion, these data demonstrate that neurulation-stage alcohol exposure decrease Shh pathway signaling, Shh-mediated cell cycle gene expression, and cilia-related gene expression in a region of the neural tube that gives rise to alcohol-sensitive ventral midline brain structures. Furthermore, NAE interacts with primary cilia to alter open field and EPM behavior in *Kif3a* mutant male mice during adolescence. NAE causes downregulation of *Shh* and alters genes related to ciliogenesis and protein trafficking within 6 hr post-exposure, which then alters Gli signaling within the cilia and decreases *Ccnd1* expression (Fig 5) and reduces RVNT volume. These studies suggest that the changes to cilia-related genes are indicative of primary cilia dysfunction resulting in abnormal Shh pathway signaling similar to many genetic ciliopathies. Together, this demonstrates an interaction of prenatal alcohol and primary cilia, particularly in relation to midline craniofacial and CNS defects, resulting in an alcohol-induced “transient ciliopathy”.

Acknowledgements

We thank you to Jamie Leitzinger, Divya Venkatasubramanian, Haley Mendoza-Romero, Laura Murdaugh, and Debbie Dehart for their technical assistance on this project.

Competing interests

The authors have no conflicts of interest to report.

Funding

Funding to support this research was provided by the National Institutes of Health/National Institute of Alcohol and Alcoholism [U01AA021651 and R01AA026068 to SEP, F32AA026479 to KEB] and conducted as part of the Collaborative Initiative on Fetal Alcohol Spectrum Disorders (CIFASD).

Author Contributions

Conceptualization: KEB, EWF, and SEP
Methodology: KEB, EWF, and SEP
Investigation: KEB and EWF
Formal Analysis: KEB and EWF
Visualization: KEB and EWF
Writing – Original Draft Preparation: KEB and EWF
Writing – Review & Editing: KEB, EWF, and SEP

References

1. May PA, Chambers CD, Kalberg WO, Zellner J, Feldman H, Buckley D, et al. Prevalence of fetal alcohol spectrum disorders in 4 US communities. JAMA. 2018;319(5):474-82.
2. Cook CS, Nowotny AZ, Sulik KK. Fetal alcohol syndrome: eye malformations in a mouse model. Archives of Ophthalmology. 1987;105(11):1576-81.
3. Godin EA, O'Leary-Moore SK, Khan AA, Parnell SE, Ament JJ, Dehart DB, et al. Magnetic Resonance Microscopy Defines Ethanol-Induced Brain Abnormalities in Prenatal Mice: Effects of Acute Insult on Gestational Day 7. Alcoholism: Clinical and Experimental Research. 2010;34(1):98-111.
4. Suttie M, Wetherill L, Jacobson SW, Jacobson JL, Hoyme HE, Sowell ER, et al. Facial curvature detects and explicates ethnic differences in effects of prenatal alcohol exposure. Alcoholism: Clinical and Experimental Research. 2017.
5. Dunty WC, Chen Sy, Zucker RM, Dehart DB, Sulik KK. Selective Vulnerability of Embryonic Cell Populations to Ethanol-Induced Apoptosis: Implications for Alcohol-Related Birth Defects and Neurodevelopmental Disorder. Alcoholism: Clinical and Experimental Research. 2001;25(10):1523-35.
6. Kietzman HW, Everson JL, Sulik KK, Lipinski RJ. The teratogenic effects of prenatal ethanol exposure are exacerbated by Sonic Hedgehog or GLI2 haploinsufficiency in the mouse. PloS one. 2014;9(2):e89448.
7. Smith SM, Garic A, Flentke GR, Berres ME. Neural crest development in fetal alcohol syndrome. Birth Defects Research Part C: Embryo Today: Reviews. 2014;102(3):210-20.
8. Aoto K, Shikata Y, Higashiyama D, Shiota K, Motoyama J. Fetal ethanol exposure activates protein kinase A and impairs Shh expression in prechordal mesendoderm cells in the pathogenesis of holoprosencephaly. Birth Defects Research Part A: Clinical and Molecular Teratology. 2008;82(4):224-31.
9. Zhang C, Frazier JM, Chen H, Liu Y, Lee JA, Cole GJ. Molecular and morphological changes in zebrafish following transient ethanol exposure during defined developmental stages. Neurotoxicol Teratol. 2014;44:70-80.
10. Higashiyama D, Saitsu H, Komada M, Takigawa T, Ishibashi M, Shiota K. Sequential developmental changes in holoprosencephalic mouse embryos exposed to ethanol during the gastrulation period. Birth defects research Part A, Clinical and molecular teratology. 2007;79(7):513-23.
11. Fish E, Holloway H, Rumple A, Baker L, Wieczorek L, Moy S, et al. Acute alcohol exposure during neurulation: Behavioral and brain structural consequences in adolescent C57BL/6J mice. Behavioural brain research. 2016;311:70-80.
12. Parnell SE, Holloway HT, O'Leary-Moore SK, Dehart DB, Paniaqua B, Oguz I, et al. Magnetic resonance microscopy-based analyses of the neuroanatomical effects of gestational day 9 ethanol exposure in mice. Neurotoxicology and teratology. 2013;39:77-83.
13. Parnell SE, O'Leary-Moore SK, Godin EA, Dehart DB, Johnson BW, Allan Johnson G, et al. Magnetic Resonance Microscopy Defines Ethanol-Induced Brain Abnormalities in Prenatal Mice: Effects of Acute Insult on Gestational Day 8. Alcoholism: Clinical and Experimental Research. 2009;33(6):1001-11.
14. Cortés CR, Metzis V, Wicking C. Unmasking the ciliopathies: craniofacial defects and the primary cilium. Wiley Interdisciplinary Reviews: Developmental Biology. 2015;4(6):637-53.
15. Gerdes JM, Davis EE, Katsanis N. The Vertebrate Primary Cilium in Development, Homeostasis, and Disease. Cell. 2009;137(1):32-45.
16. Abdelhamed ZA, Wheway G, Szymanska K, Natarajan S, Toomes C, Inglehearn C, et al. Variable expressivity of ciliopathy neurological phenotypes that encompass Meckel–Gruber syndrome and Joubert syndrome is caused by complex de-regulated ciliogenesis, Shh and Wnt signalling defects. Human molecular genetics. 2013:dds546.
17. Waters AM, Beales PL. Ciliopathies: an expanding disease spectrum. Pediatric Nephrology. 2011;26(7):1039-56.

18. Alby C, Piquand K, Huber C, Megarbané A, Ichkou A, Legendre M, et al. Mutations in KIAA0586 cause lethal ciliopathies ranging from a hydrolethalus phenotype to short-rib polydactyly syndrome. The American Journal of Human Genetics. 2015;97(2):311-8.
19. Shaheen R, Shamseldin HE, Loucks CM, Seidahmed MZ, Ansari S, Khalil MI, et al. Mutations in CSPP1, encoding a core centrosomal protein, cause a range of ciliopathy phenotypes in humans. The American Journal of Human Genetics. 2014;94(1):73-9.
20. Cortellino S, Wang C, Wang B, Bassi MR, Caretti E, Champeval D, et al. Defective ciliogenesis, embryonic lethality and severe impairment of the Sonic Hedgehog pathway caused by inactivation of the mouse complex A intraflagellar transport gene Ift122/Wdr10, partially overlapping with the DNA repair gene Med1/Mbd4. Developmental biology. 2009;325(1):225-37.
21. Stottmann R, Tran P, Turbe-Doan A, Beier DR. Ttc21b is required to restrict sonic hedgehog activity in the developing mouse forebrain. Developmental biology. 2009;335(1):166-78.
22. Tran PV, Haycraft CJ, Besschetnova TY, Turbe-Doan A, Stottmann RW, Herron BJ, et al. THM1 negatively modulates mouse sonic hedgehog signal transduction and affects retrograde intraflagellar transport in cilia. Nature genetics. 2008;40(4):403-10.
23. Brugmann SA, Allen NC, James AW, Mekonnen Z, Madan E, Helms JA. A primary cilia-dependent etiology for midline facial disorders. Human molecular genetics. 2010;19(8):1577-92.
24. Brugmann S, Chang C-F, Millington G. GLI-dependent Etiology of Craniofacial Ciliopathies. The FASEB Journal. 2015;29(1_supplement):86.2.
25. Chang C-F, Chang Y-T, Millington G, Brugmann SA. Craniofacial ciliopathies reveal specific requirements for GLI proteins during development of the facial midline. PLoS genetics. 2016;12(11):e1006351.
26. O'Leary-Moore SK, Parnell SE, Godin EA, Dehart DB, Ament JJ, Khan AA, et al. Magnetic resonance microscopy-based analyses of the brains of normal and ethanol-exposed fetal mice. Birth Defects Research Part A: Clinical and Molecular Teratology. 2010;88(11):953-64.
27. Schindelin J, Arganda-Carreras I, Frise E, Kaynig V, Longair M, Pietzsch T, et al. Fiji: an open-source platform for biological-image analysis. Nature methods. 2012;9(7):676-82.
28. Osborn J, Yu C, Gabriel K, Weinberg J. Fetal ethanol effects on benzodiazepine sensitivity measured by behavior on the elevated plus-maze. Pharmacology Biochemistry and Behavior. 1998;60(3):625-33.
29. File SE. Factors controlling measures of anxiety and responses to novelty in the mouse. Behavioural brain research. 2001;125(1-2):151-7.
30. Fish E, Wieczorek L, Parnell S. Neurobehavioral Consequences Of Early Gestational Binge-like Alcohol Exposure: Age-related Alterations In Male And Female C57bu6j Mice. Alcoholism: Clinical & Experimental Research. 2015;39:165A.
31. Livak KJ, Schmittgen TD. Analysis of relative gene expression data using real-time quantitative PCR and the $2^{-\Delta\Delta CT}$ method. Methods (San Diego, Calif). 2001;25(4):402-8.
32. McDonald JH. Handbook of biological statistics: Sparky House Publishing Baltimore, MD; 2009.
33. Holson R, Pearce B. Principles and pitfalls in the analysis of prenatal treatment effects in multiparous species. Neurotoxicology and teratology. 1992;14(3):221-8.
34. Fish E, Wieczorek L, Rumple A, Suttie M, Moy S, Hammond P, et al. the enduring impact of neurulation stage alcohol exposure: A combined behavioral and structural neuroimaging study in adult male and female C57bl/6j mice. Behavioural brain research. 2018;338:173-84.
35. Wieczorek L, Fish EW, O'Leary-Moore SK, Parnell SE, Sulik KK. Hypothalamic-pituitary-adrenal axis and behavioral dysfunction following early binge-like prenatal alcohol exposure in mice. Alcohol. 2015;49(3):207-17.
36. Wilson SL, Wilson JP, Wang C, Wang B, McConnell SK. Primary cilia and Gli3 activity regulate cerebral cortical size. Developmental neurobiology. 2012;72(9):1196-212.
37. Ishibashi M, McMahon AP. A sonic hedgehog-dependent signaling relay regulates growth of diencephalic and mesencephalic primordia in the early mouse embryo. Development. 2002;129(20):4807-19.

38. Saitsu H, Komada M, Suzuki M, Nakayama R, Motoyama J, Shiota K, et al. Expression of the mouse Fgf15 gene is directly initiated by Sonic hedgehog signaling in the diencephalon and midbrain. Developmental dynamics : an official publication of the American Association of Anatomists. 2005;232(2):282-92.
39. Fischer T, Faus-Kessler T, Welzl G, Simeone A, Wurst W, Prakash N. Fgf15-mediated control of neurogenic and proneural gene expression regulates dorsal midbrain neurogenesis. Dev Biol. 2011;350(2):496-510.
40. Sherr CJ, Roberts JM. CDK inhibitors: positive and negative regulators of G1-phase progression. Genes & development. 1999;13(12):1501-12.
41. Kasper M, Schnidar H, Neill GW, Hanneder M, Klingler S, Blaas L, et al. Selective modulation of Hedgehog/GLI target gene expression by epidermal growth factor signaling in human keratinocytes. Molecular and cellular biology. 2006;26(16):6283-98.
42. Alvarez-Medina R, Le Dreau G, Ros M, Martí E. Hedgehog activation is required upstream of Wnt signalling to control neural progenitor proliferation. Development. 2009;136(19):3301-9.
43. Watson C, Paxinos G, Puelles L. The mouse nervous system: Academic Press; 2012.
44. Boschen KE, Parnell SE. Transcriptome-wide analysis in the neural tube following mid-neurulation stage ethanol exposure in C57BL/6J mice. Research Society on Alcohol Annual Meeting; San Diego, CA: Alcoholism: Clinical & Experimental Research; 2018. p. 42A.
45. Arnaiz O, Cohen J, Tassin A-M, Koll F. Remodeling Cildb, a popular database for cilia and links for ciliopathies. Cilia. 2014;3(1):9.
46. Arnaiz O, Malinowska A, Klotz C, Sperling L, Dadlez M, Koll F, et al. Cildb: a knowledgebase for centrosomes and cilia. Database. 2009;2009:bap022.
47. Keryer G, Pineda JR, Liot G, Kim J, Dietrich P, Benstaali C, et al. Ciliogenesis is regulated by a huntingtin-HAP1-PCM1 pathway and is altered in Huntington disease. The Journal of clinical investigation. 2011;121(11):4372-82.
48. Schaub JR, Stearns T. The Rilp-like proteins Rilpl1 and Rilpl2 regulate ciliary membrane content. Molecular biology of the cell. 2013;24(4):453-64.
49. Liu J-P, Zeitlin SO. The long and the short of aberrant ciliogenesis in Huntington disease. The Journal of clinical investigation. 2011;121(11).
50. Gauthier LR, Charrin BC, Borrell-Pages M, Dompierre JP, Rangone H, Cordelieres FP, et al. Huntingtin controls neurotrophic support and survival of neurons by enhancing BDNF vesicular transport along microtubules. Cell. 2004;118(1):127-38.
51. Lee JE, Silhavy JL, Zaki MS, Schroth J, Bielas SL, Marsh SE, et al. CEP41 is mutated in Joubert syndrome and is required for tubulin glutamylation at the cilium. Nature genetics. 2012;44(2):193-9.
52. Coene KL, Mans DA, Boldt K, Gloeckner CJ, van Reeuwijk J, Bolat E, et al. The ciliopathy-associated protein homologs RPGRIP1 and RPGRIP1L are linked to cilium integrity through interaction with Nek4 serine/threonine kinase. Hum Mol Genet. 2011;20(18):3592-605.
53. Zariwala M, O'Neal WK, Noone PG, Leigh MW, Knowles MR, Ostrowski LE. Investigation of the possible role of a novel gene, DPCD, in primary ciliary dyskinesia. American journal of respiratory cell and molecular biology. 2004;30(4):428-34.
54. Caparrós-Martín JA, Valencia M, Reytor E, Pacheco M, Fernandez M, Perez-Aytes A, et al. The ciliary Evc/Evc2 complex interacts with Smo and controls Hedgehog pathway activity in chondrocytes by regulating Sufu/Gli3 dissociation and Gli3 trafficking in primary cilia. Human molecular genetics. 2012;22(1):124-39.
55. Dorn KV, Hughes CE, Rohatgi R. A Smoothened-Evc2 complex transduces the Hedgehog signal at primary cilia. Developmental cell. 2012;23(4):823-35.
56. Kotch L, Dehart D, Alles A, Chernoff N, Sulik K. Pathogenesis of ethanol-induced limb reduction defects in mice. Teratology. 1992;46(4):323-32.

57. McMechan AP, O'Leary-Moore SK, Morrison SD, Hannigan JH. Effects of prenatal alcohol exposure on forepaw digit length and digit ratios in rats. Developmental psychobiology. 2004;45(4):251-8.
58. Jones K, Smith D. Recognition of the fetal alcohol syndrome in early infancy. The Lancet. 1973;302(7836):999-1001.
59. Liu B, Chen S, Johnson C, Helms J. A ciliopathy with hydrocephalus, isolated craniosynostosis, hypertelorism, and clefting caused by deletion of Kif3a. Reproductive Toxicology. 2014;48:88-97.
60. Lehti MS, Kotaja N, Sironen A. KIF3A is essential for sperm tail formation and manchette function. Molecular and cellular endocrinology. 2013;377(1):44-55.
61. Parnell SE, Holloway HE, Baker LK, Styner MA, Sulik KK. Dysmorphogenic effects of first trimester-equivalent ethanol exposure in mice: A magnetic resonance microscopy-based study. Alcoholism: Clinical and Experimental Research. 2014;38(7):2008-14.
62. Bailey JM, Singh PK, Hollingsworth MA. Cancer metastasis facilitated by developmental pathways: Sonic hedgehog, Notch, and bone morphogenic proteins. Journal of cellular biochemistry. 2007;102(4):829-39.
63. Michaud EJ, Yoder BK. The primary cilium in cell signaling and cancer. Cancer research. 2006;66(13):6463-7.
64. Ding Q, Motoyama J, Gasca S, Mo R, Sasaki H, Rossant J, et al. Diminished Sonic hedgehog signaling and lack of floor plate differentiation in Gli2 mutant mice. Development. 1998;125(14):2533-43.
65. Matise MP, Epstein DJ, Park HL, Platt KA, Joyner AL. Gli2 is required for induction of floor plate and adjacent cells, but not most ventral neurons in the mouse central nervous system. Development. 1998;125(15):2759-70.
66. Park H, Bai C, Platt K, Matise M, Beeghly A, Hui C, et al. Mouse Gli1 mutants are viable but have defects in SHH signaling in combination with a Gli2 mutation. Development. 2000;127(8):1593-605.
67. Hong S-R, Wang C-L, Huang Y-S, Chang Y-C, Chang Y-C, Pusapati GV, et al. Spatiotemporal manipulation of ciliary glutamylation reveals its roles in intraciliary trafficking and Hedgehog signaling. Nature communications. 2018;9.
68. Takeda S, Yonekawa Y, Tanaka Y, Okada Y, Nonaka S, Hirokawa N. Left-right asymmetry and kinesin superfamily protein KIF3A: new insights in determination of laterality and mesoderm induction by kif3A−/− mice analysis. The Journal of cell biology. 1999;145(4):825-36.
69. Dafinger C, Liebau MC, Elsayed SM, Hellenbroich Y, Boltshauser E, Korenke GC, et al. Mutations in KIF7 link Joubert syndrome with Sonic Hedgehog signaling and microtubule dynamics. The Journal of clinical investigation. 2011;121(7):2662-7.
70. Astley SJ, Clarren SK. Measuring the facial phenotype of individuals with prenatal alcohol exposure: correlations with brain dysfunction. Alcohol and alcoholism (Oxford, Oxfordshire). 2001;36(2):147-59.

Supporting information

S1 Fig. Uncropped western blot analysis of Gli3. A) GD9.25 (6 hr post-exposure) blot of Gli3 full length (190 kDa), cleaved (83 kDA), and Gapdh (37 kDa) bands. B) GD9.5 blot of Gli3 and Gapdh. NAE: Neurulation-stage alcohol exposure; Veh: Lactated Ringer's vehicle group. Each lane represents one pooled litter from the treatment group indicated.

S2 Fig. NAE causes impairments in rotarod performance in male, but not female, mice. Male NAE mice, regardless of genotype, had a significantly shorter latency to fall compared to vehicle-treated mice ($F_{(1,48)} = 5.1$; $p = 0.028$). No effect of genotype or treatment on rotarod performance was found in female mice. A main effect of trial was found ($F_{(4,220)} = 24.46$, $p < 0.0001$), demonstrating motor learning in the females across trials. * = $p < 0.05$. For males, n's = 11-15 litters; for females, n's = 13-17 litters. Data are shown as group means ± SEM with each sample representing littermates of each genotype averaged into a single datum.

S3 Fig. Partial loss of cilia motor transport gene *Kif3a* affects behavioral performance on the EPM (A-C) and open field (D-F) in adolescent female mice. For EPM, total arm entries (A) and percent of time (B) in open arms showed no effects of treatment or genotype. However, C) a significant main effect of genotype was revealed for percent of entries into open arms ($F_{(1, 57)} = 5.13$, $p = 0.028$), with *Kif3a*$^{+/-}$ female mice making more entries into open arms compared to WT mice. For open field, there was a significant genotype effect (indicated by curved brackets) on horizontal activity (D) ($F_{(1,54)} = 9.2$, $p = 0.004$), center distance (E) ($F_{(1,54)} = 7.9$, $p = 0.007$), center time (F) ($F_{(1,54)} = 6.4$; $p = 0.014$), and repeated beam breaks (data not shown) ($F_{(1,54)} = 6.7$; $p = 0.013$). Overall, when all time bins were averaged, *Kif3a*$^{+/-}$ female mice were more active and traveled farther in the center of the open field compared to WT females. *Post hoc* analyses were not significant. * = $p < 0.05$, ** = $p < 0.01$. When data were totaled across the session (D-F), Bonferroni *post hoc* tests revealed that Veh *Kif3a*$^{+/-}$ mice had more beam breaks ($p = 0.005$) and center distance traveled ($p = 0.003$) compared to Veh WT mice. For totaled data, significant ($p < 0.05$) *post hoc*'s are shown as letters on each graph. a: vs. vehicle-treated WT, b: vs. vehicle-treated *Kif3a*$^{+/-}$, c: vs. NAE WT. For all groups, n's = 13-17 litters. All data are shown as group means ± SEM with each sample representing the females from one litter.

S4 Fig. Partial loss of *Kif3a* reduces brain width and height in adolescent male mice. A) Neither genotype nor prenatal treatment affected ventricle area. However, B) midline brain width was smaller in both *Kif3a*$^{+/-}$ groups and NAE WT animals compared to vehicle-treated WT mice. C) *Kif3a* heterozygosity also results in smaller medial brain height. * = $p < 0.05$, ** = $p < 0.01$, *** = $p < 0.001$. Group n's = 4-5. All measurements shown as mean + SEM.

S1 Table. Open field behavioral outcomes in adolescent male *Kif3a*$^{+/-}$ and *Kif3a*$^{+/+}$ mice following NAE or vehicle treatment on GD9.0.

S2 Table. Open field behavioral outcomes in adolescent female *Kif3a*$^{+/-}$ and *Kif3a*$^{+/+}$ mice following NAE or vehicle treatment on GD9.0. [a] = Veh *Kif3a*$^{+/-}$ and NAE *Kif3a*$^{+/-}$ (averaged across time bins) significantly differ from the average of Veh WT.

Figure 1.

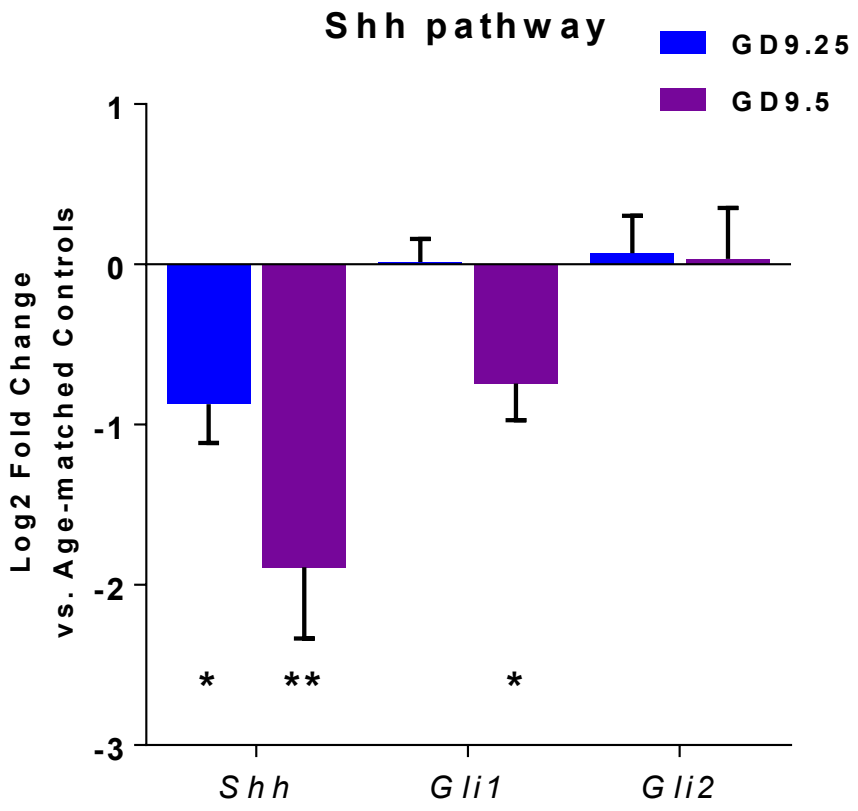
A
Shh pathway
GD9.25
GD9.5
Log2 Fold Change
vs. Age-matched Controls
1
0
-1
-2
-3
*
**
*
Shh
Gli1
Gli2

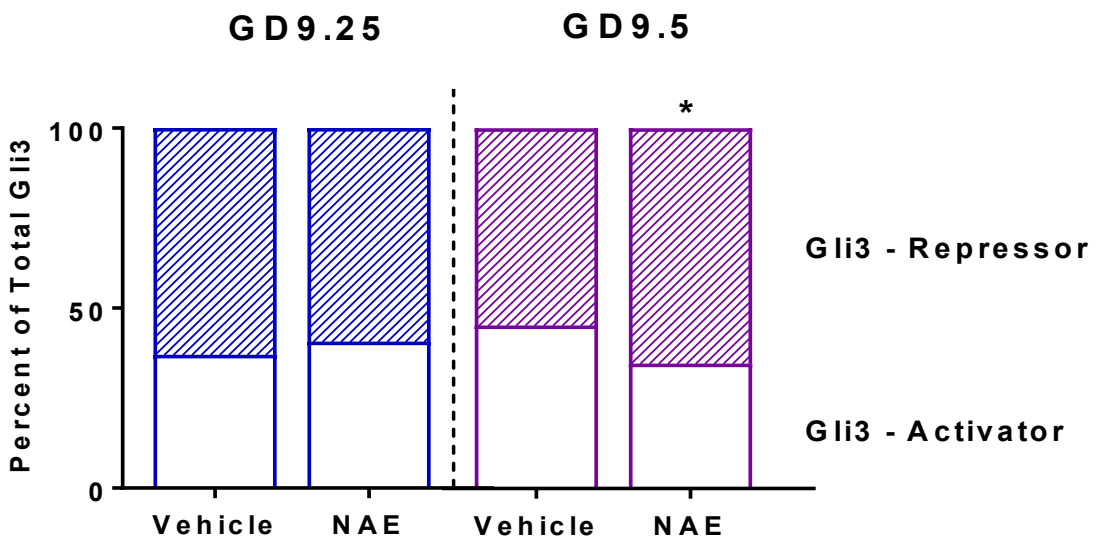
B
GD9.25
GD9.5
Percent of Total Gli3
100
50
0
*
Gli3 - Repressor
Gli3 - Activator
Vehicle
NAE
Vehicle
NAE

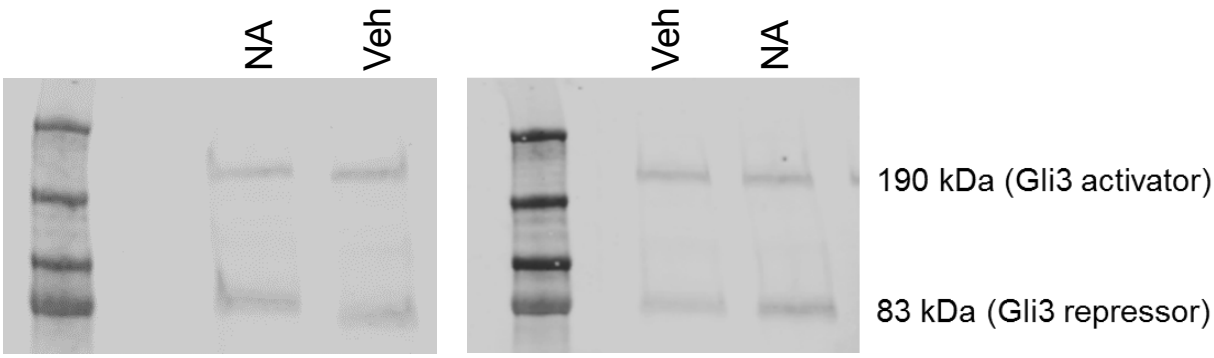
NA
Veh
Veh
NA
190 kDa (Gli3 activator)
83 kDa (Gli3 repressor)

Figure 2.

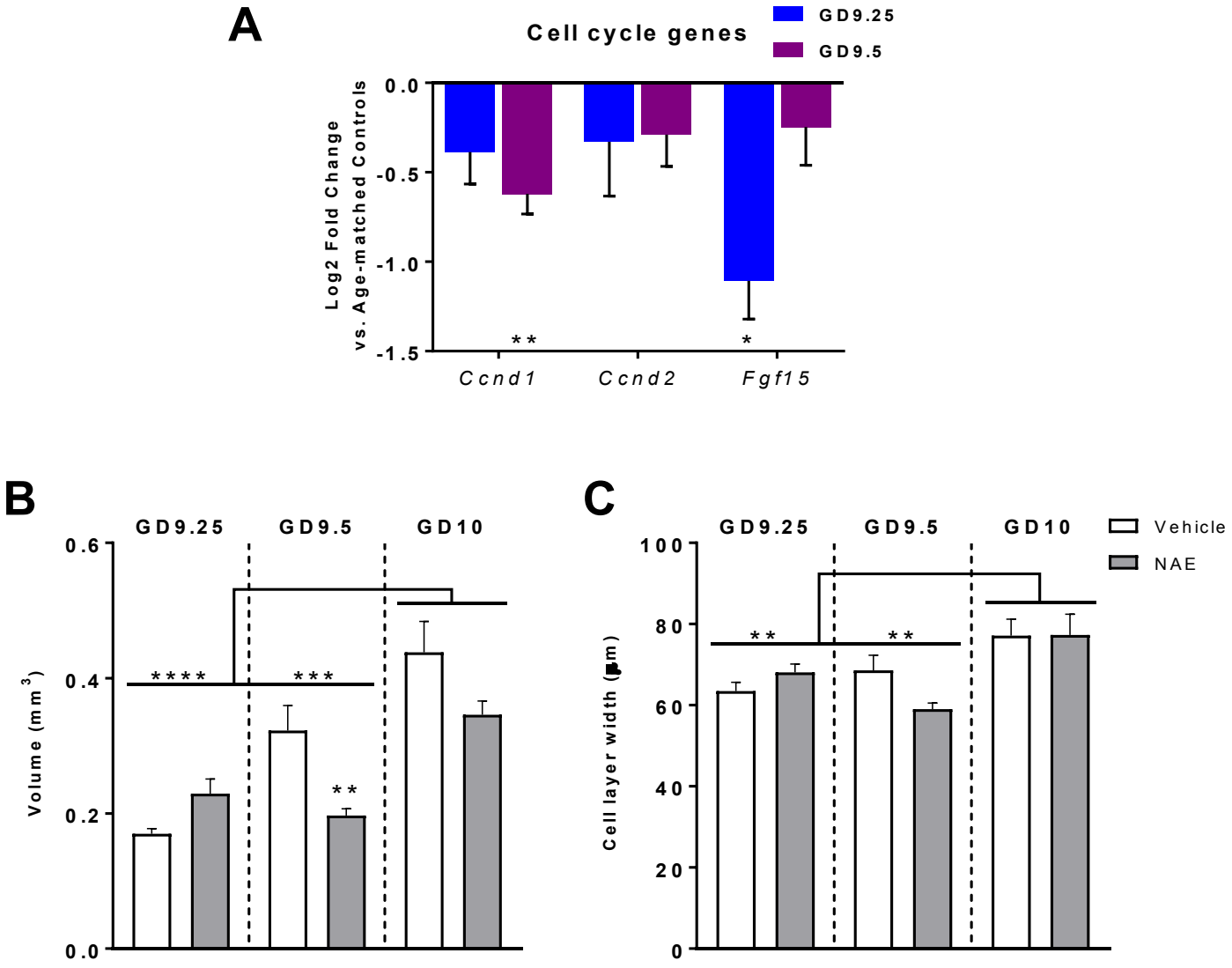
A
Cell cycle genes
GD9.25
GD9.5
Log2 Fold Change
vs. Age-matched Controls
0.0
-0.5
-1.0
-1.5
**
*
Ccnd1
Ccnd2
Fgf15
B
GD9.25
GD9.5
GD10
Volume (mm3)
0.6
0.4
0.2
0.0
****
***
**
C
GD9.25
GD9.5
GD10
Vehicle
NAE
Cell layer width (µm)
100
80
60
40
20
0
**
**

Figure 3.

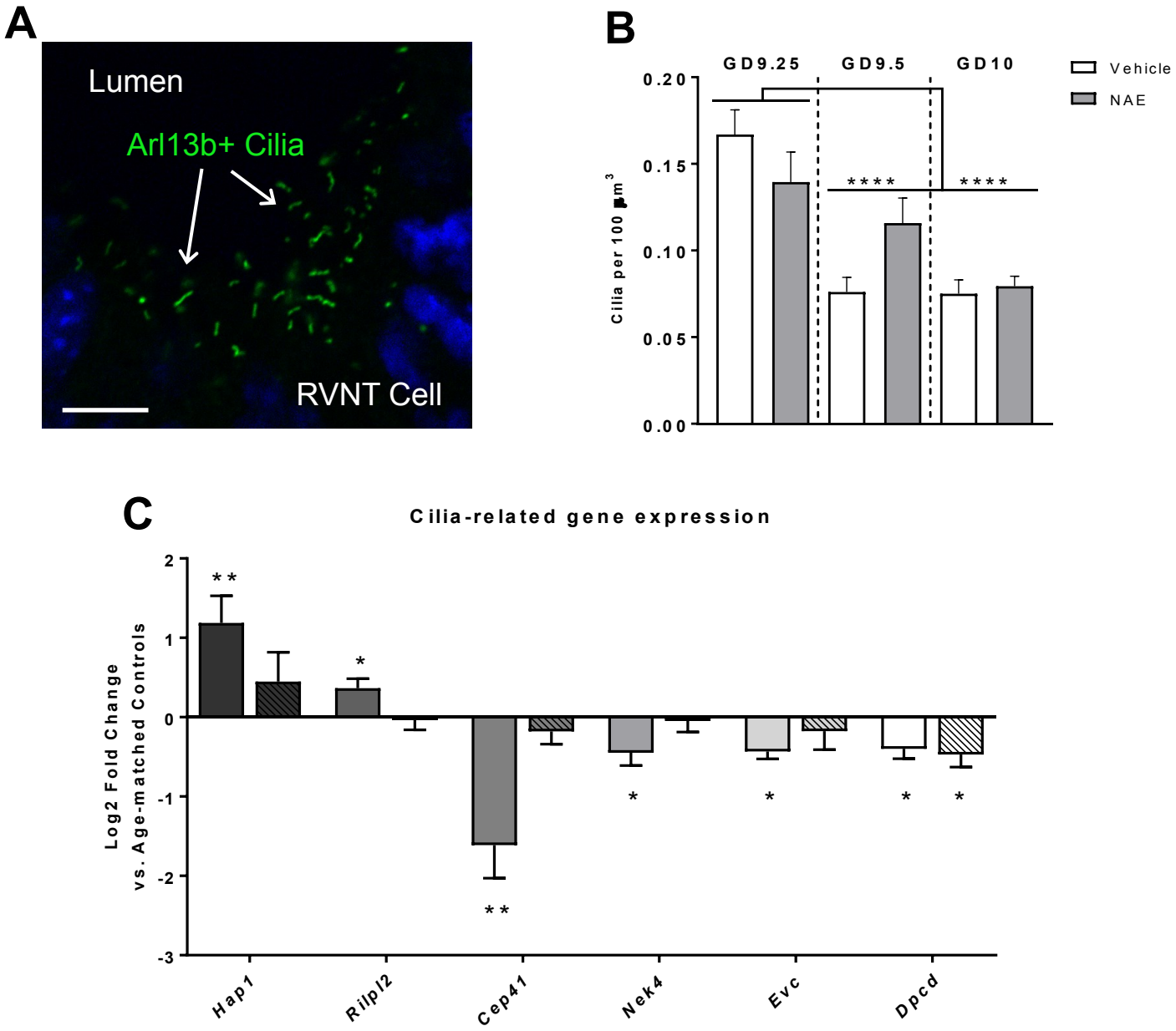
A
Lumen
Arl13b+ Cilia
RVNT Cell
B
GD9.25
GD9.5
GD10
Vehicle
NAE
Cilia per 100 μm3
0.20
0.15
0.10
0.05
0.00
****
****
C
Cilia-related gene expression
Log2 Fold Change vs. Age-matched Controls
2
1
0
-1
-2
-3
**
*
**
*
*
*
*
Hap1
Rilpl2
Cep41
Nek4
Evc
Dpcd

Figure 4.

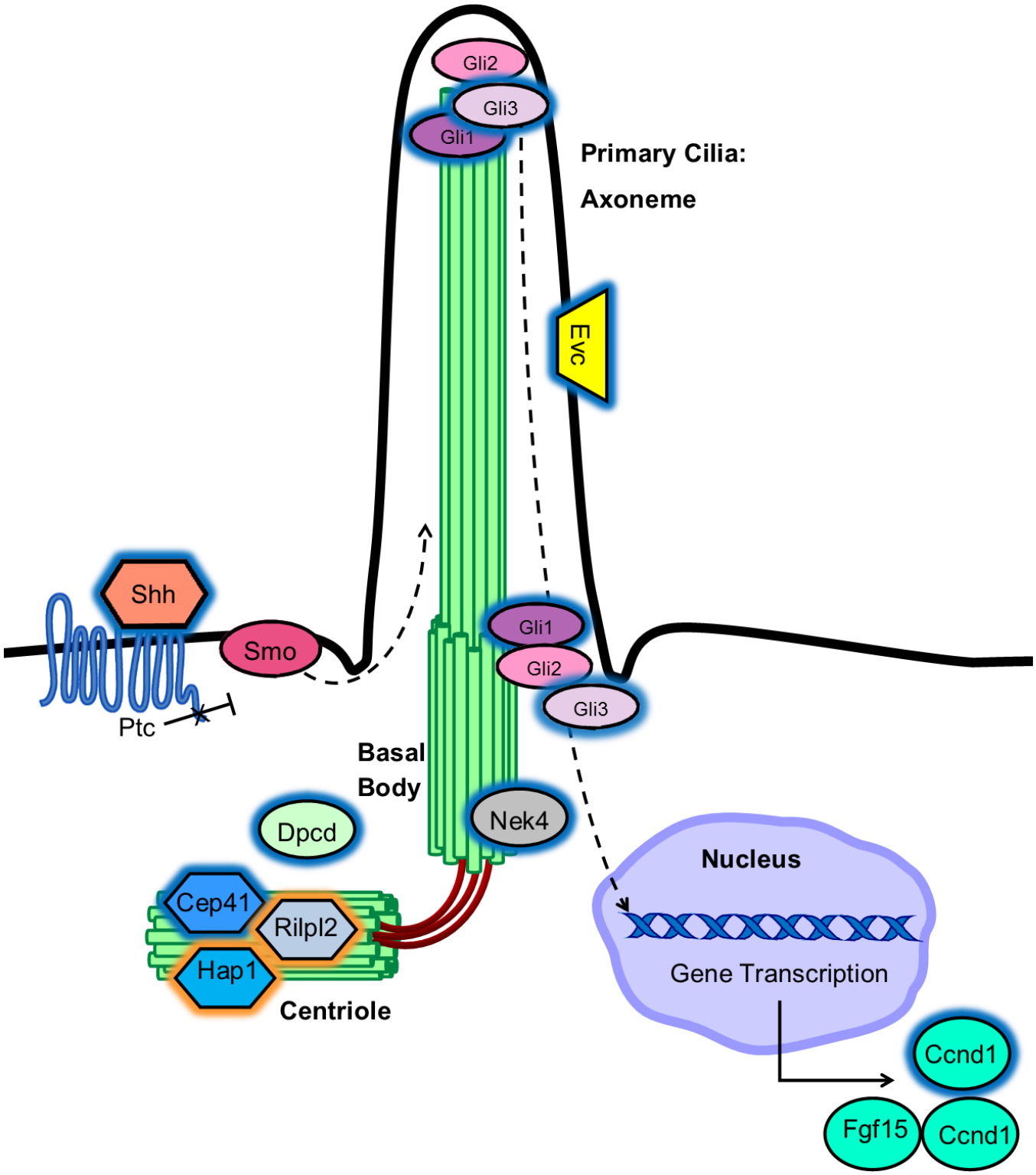
Gli2
Gli3
Gli1
Primary Cilia:
Axoneme
Evc
Shh
Smo
Ptc
Gli1
Gli2
Gli3
Basal
Body
Nek4
Dpcd
Cep41
Rilpl2
Hap1
Centriole
Nucleus
Gene Transcription
Ccnd1
Fgf15
Ccnd1

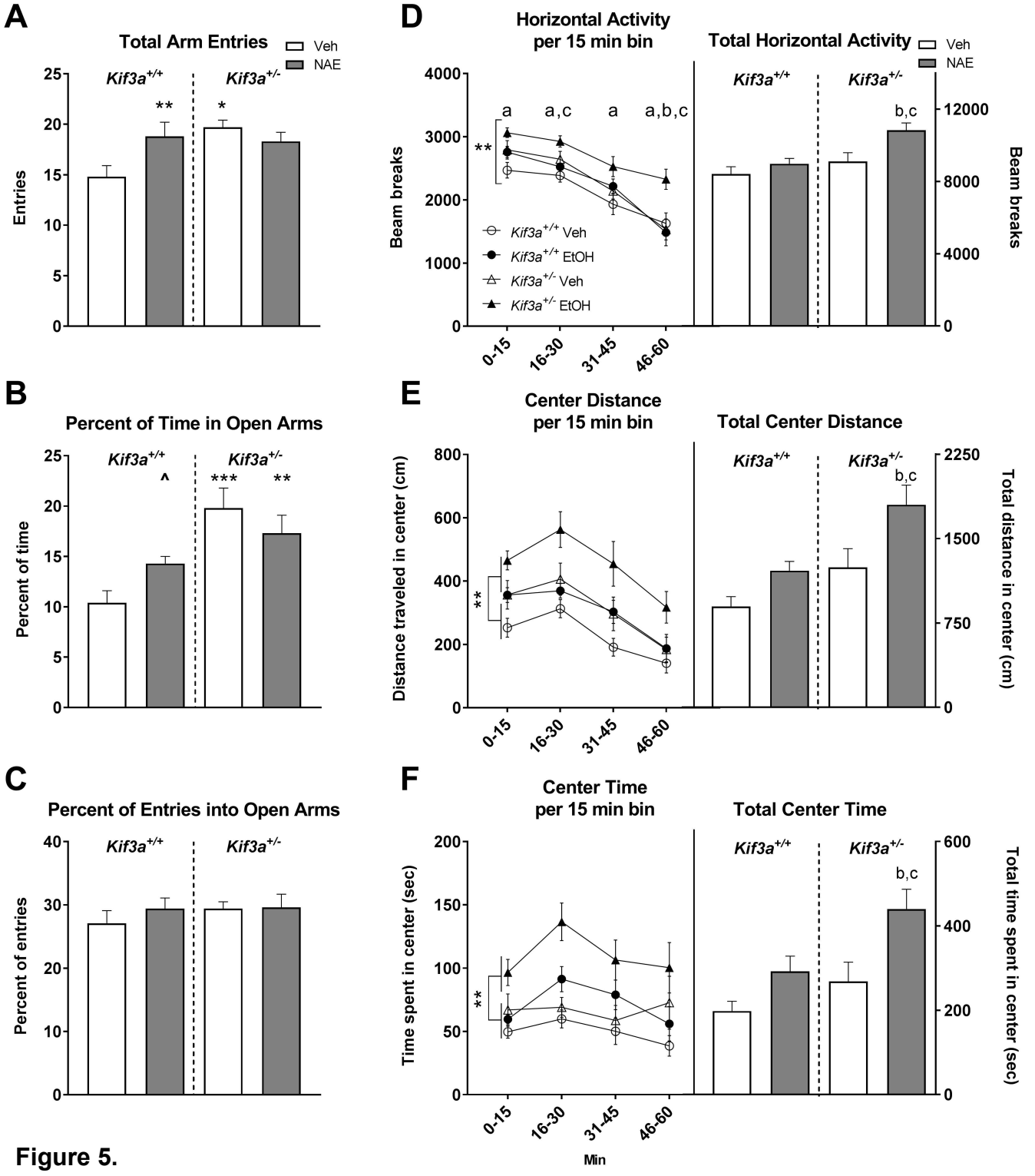
A
Total Arm Entries
Veh
NAE
Kif3a+/+
Kif3a+/-
Entries
B
Percent of Time in Open Arms
Percent of time
C
Percent of Entries into Open Arms
Percent of entries
D
Horizontal Activity per 15 min bin
Total Horizontal Activity
Beam breaks
Kif3a+/+ Veh
Kif3a+/+ EtOH
Kif3a+/- Veh
Kif3a+/- EtOH
0-15
16-30
31-45
46-60
E
Center Distance per 15 min bin
Total Center Distance
Distance traveled in center (cm)
Total distance in center (cm)
F
Center Time per 15 min bin
Total Center Time
Time spent in center (sec)
Total time spent in center (sec)
Min

Figure 5.